Light Extraction Efficiency Analysis of Phosphorescent OLED Device with Microlens Array on the Glass Substrate

Arvind Sharma

NITAP: National Institute of Technology Arunachal Pradesh

T. D. Das (✉ tddas@hotmail.com)

National Institute of Technology Arunachal Pradesh

Abstract

The Computational simulation is based on the desired packing type of microlens array, either hexagonal or rectangular, onto the planar dual scheme OLED device's light-emitting surface. Both active layers here acted as a phosphorescent emission layer studied to improve device efficiency. The microlens array (MLAs) with hexagonal packing can increase the external quantum efficiency by 35%, which is more than the literature mentioned earlier. It significantly enhances the outcoupling efficiency below the critical angle observation concerning the substrate surface normal. Besides, a broad spectrum is observed with a slight shoulder band around 650 nm in the E.L. (Electroluminance) emission curve. From the CIE x and CIE y index studied, the OLED device connected with either hexagonal or rectangular microlens arrays are more sensitive than the OLED device without microlens arrays to the viewing angle range. The effect of outcoupled efficiency as a function of ETL-TPBi thickness is studied under different polarization modes. Hence, the study suggested that a microlens array with a hexagonal or rectangular packing type on the OLED device's top significantly enhanced light extraction efficiency and provided better device fabrication results.

1. Introduction

Organic light-emitting diodes (OLEDs) have become a potential candidate in the field of the next-generation planar light source due to the following features such as light-weight, low thickness, and energy-saving source, which is economically favorable in comparison with an inorganic light-emitting diode [1]. Several OLEDs have been successfully introduced in the global market for many lighting display applications. But still, higher outcoupling of light on the glass-air interface and the longer lifetime remains a bottleneck in OLED devices' performance and becomes a concerning issue among the researcher [2, 3]. Because more than 80% of light is lost due to the combined effect of total internal reflection (TIR) and waveguiding at boundaries of different refractive index materials [4, 5, 6]. Several literature methods such as the microporous polymer [7–9], the microlens array (MLAs) [10] have been proposed to counter the problem of light extraction efficiency by inserting the array onto the glass substrate. Because they don't induce any alteration either in the architecture of the device or in the functioning, these micropatterns onto the glass substrate only change the path of light propagation, resulting in the reduction of waveguide mode and an enhancement in external mode [10]. However, in the processing of large-area substrates, MLAs' fabrication is easy and efficient [11]. Simultaneously, the other primary concern is the imperfection limit in the generation of light in the active layer, mainly due to charge imbalance. It can be overcome using a hole modulating layer between HTL/EML or EML/ETL to obtain balanced carrier injection into the active layer. Hence, its reduced charge imbalance and enhanced hole injection rate [12, 13]. Thus, for a higher recombination rate, the attribution of a dual phosphorescent function-based active layer is used to intensify the exciton operation. Among the previous research, there are several papers reported to obtain a highly efficient OLED device using a multi-active layer [14, 15] and stated to achieved the highest EQE by 30% [15]. While the OLED with MLAs has achieved the highest EQE by 34% [16]. Therefore, for higher outcoupling efficiency, optimization is essential before the fabrication

of the device. This article aims to enhance the light extraction efficiency by using different micropattern arrays onto the dual scheme OLED device's glass substrate. Therefore, we used commercially available software tools to perform such operations that make such calculations using optical dipole models and 3D ray-tracing models, respectively.

2. Proposed Oled Design Structure And Microlens Array Packing Type

The OLED device comprises a set of thin organic layers with a specific function in the overall device. The organic layer employed over ITO (indium tin oxide) with a thickness of 120 nm acts as an anode because of a high work function and reflectivity, and aluminum (Al-150 nm) acts as a cathode due to high reflectance over the visible wavelength. The used ultrathin organic materials are TAPC (4,4' - cyclohexylidenebis [N, N-bis(4-methylphenyl) benzenamine]) as a hole transport layer (HTL-40 nm), and TPBi (2, 2', 2" - (1,3,5-Benzinetriyl)-tris(1-phenyl-1-H-benzimidazole)) as an electron transport layer (ETL-50 nm). Here,we used dual scheme of active layer which function as phosphorescent layer namely α- NPD:Ir $(MDQ)_2$ as EMI1 [N, N' Di(1-naphthyl)-N, N'-diphenyl-(1,1'-bipheny)-4,4'-diamine doped with the red-emitting dye bis (2-methyldibenzo[f, h]quinoxaline)(acetylacetonate)iridium(III)], TCTA: $Ir(ppy)_3$ as EML2 [tris(4-carbazoyl-9-ylphenyl)amine] doped with the green-emitting dye tris[2-phenylpyridinato-C2,N] iridium(III)]. In this emission layer EML1 the HTM (hole transport material), α-NPD, as a host material and $Ir(MDQ)_2$ as a guest material.

Similarly, in EML2, the HTM, TCTA, as a host material and $Ir(ppy)_3$ as a guest material [17]. The simulation tools **SETFOS 5.0.6** used the 3D Ray-tracing method based on the geometric optic to calculate an interface's scattering properties. Where we predefined, geometry patterned onto glass substrate and detail of used dimensions are listed in Table I. The packing types for the microlens array are rectangular and hexagonal. The SETFOS commercially available software package was used to study the electrical and optical features of the OLED device.

Table 1. Detail of used parameter of micropatterns onto the glass substrate.

Array detail	Rectangular MLA	Hexagonal MLA
R_{lens}	10 μm	10 μm
R_{pack}	15 μm	10 μm
Height	10 μm	10 μm

Note: R_{lens} radii of the microlens array. The packing type of used microlens arrays is either hexagonal and rectangular. The ultrathin organic layer parameter used thickness value for OLED attached with microlens array is the same, i.e., ITO (120 nm)/TAPC (40 nm)/EML1(30 nm)/EML2 (30 nm)/TPBi (50 nm)/Al (150 nm).

Fig. 1(a) displays the pictorial representation of a dual scheme OLED device with microlens array as an external scattering structure. The number of photons is generated in the active layer after activating voltage across the OLED device's contacts, which causes the injection of holes from an anode and electrons from a cathode. The generated light comes out from the device through a glass substrate. However, due to the significant difference in refractive index between air (n =1.0), glass (n ≈ 1.5), and organic layers (n ≈ 1.7 − 1.9), only a tiny part of the light can leave the junction and radiate colored light from the device in the planar OLED device. Thus, to enhance the device's efficiency, TIR at the substrate/air interface must be mitigated. Therefore, we have used the microlens array as an external scattering structure onto the planar dual scheme OLED device's light-emitting surface, see fig. 1(a). Because they don't induce any alteration either in the architecture of the device or in the functioning. However, these micropatterns onto the glass substrate only change the path of light propagation, which results in the reduction of waveguide mode and an enhancement in external mode. Fig. 1(b) displays the three-dimensional view of the microlens array (rectangular); the green lines reflect the outgoing rays, and the blue lines reflect the incident rays [18, 19, 20].

3. Results And Discussion

Figure 2(a) displays a multilayer OLED device's energy level alignment diagram, including the LUMO and HOMO energies. A dc bias voltage 7 V applied across the OLED device's contacts, which causes an electron's injection from the cathode and hole from the anode, see fig. 1(a). As a result, electrons and holes' movement occurs via the hooping mechanism (because organic molecules exhibit weak van der wall force). Therefore, the accumulation of electrons and holes are observed at both sides of the active layer interface because of the difference in the organic molecule's energy barrier [13, 21]. These electrons and holes are recombined to form excitons, a coulombically bound form of electron-hole pair, and their recombination profile, see fig. 2(b). It has been observed that the three radiative recombination peaks are located at the interface and within the active layer interface. The HTL/EML1 interface, because of the low HOMO energy barrier (0.3 eV), can still effectively move the holes from the TAPC to the EML1. Besides, the LUMO barrier (0.45 eV) inhibits fewer electrons. As a result, a small peak was observed at the HTL/EML interface. But there is also energy level misalignment within the EML with HOMO energy barrier (0.22 eV), leading to a second peak within two active layer interfaces. At the EML/ETL interface, the non-reacted holes can be blocked and accrued by the 0.25 eV HOMO energy gap and encounter the electrons injected from the cathode and ETL. Hence, at EML2 / ETL interface exhibits the second-highest recombination peak. However, these formed excitons within the active layer are decay via either singlet/triplet transition and release energy in the form of photons. An average 10^{23} cm^{-3}s^{-1} recombination of electron and hole observed in the active layer. Which directly affects device performance parameters EQE [3].

The integrated luminance as a function of array height is illustrated in fig. 3(a). The result showed that integrated luminance increases monotonically with the array's height, see fig. 3(a). Incomparable to rectangular arrays, the hexagonal shape array exhibits the highest luminance due to well-controlled

geometry. As aspect ratio proportional to the height and width of the array. Thus, a higher aspect ratio has a higher intensity of light source [22]. Therefore, we are in the following results. Firstly, luminescence's high value is mainly due to using the array as an external scattering structure. Secondary, micropatterns help extract the higher light to improve the light outcoupling efficiency of OLED devices that would otherwise remain trapped inside the substrate. Tertiary, packing, and arrays are also the monitoring factors for outcoupling efficiency [23]. Fig. 3(b) shows the angular dependent radiant intensity profile of the OLED device attached with either hexagonal or rectangular shape microlens array measured at wavelength 550 nm. The angular-dependent radiance was measured to determine the exact fraction of horizontal and vertical dipoles. In the viewing angle range from ±25^0 for hexagonal while ±45^0 for rectangular, the maximum emission was observed [19]. The optical properties, therefore, vary significantly in terms of the wavelength of the emitted light. Fig. 3(c) shows the angular-dependent luminance enhancement (luminance with MLA- luminance without MLA) of the OLED device (see Table II). This angular-dependent luminance suggests that it is a Lambertian-like light source. The device luminance enhancement also decreased with an increase in the viewing angles when the hexagonal or the rectangular microlens array was positioned on the same side. The hexagonal microlenses array significantly enhances the outcoupling efficiency below the critical angle observation concerning the substrate surface normal [20, 24, 25].

TABLE II. Luminance comparison with/without a hexagonal or rectangular microlens array at different viewing angles.

Viewing angle (degree)	Luminance (Cd/m^2)			Luminance Enhancement (Cd/m^2)	
	(w/o array)	Rectangular array	Hexagonal array	Rectangular array	Hexagonal array
30^0	2064	12913	16470	10849	14406
60^0	1536	9717	9262	8181	7726

It is notably from table II; a low value of luminance is observed without any micro pattern onto the glass substrate (the chosen thickness configuration, ITO (120 nm)/TAPC (40 nm)/EML1(200 nm)/EML2 (50 nm)/TPBi (50 nm)/Al (150 nm)). In contrast, a significant enhancement in luminance was observed in the hexagonal microlens array.

The spectral extraction efficiency of the OLED device enhances significantly by employing the hexagonal or rectangular microlens array on the top of OLED, and their variation with wavelength as shown in fig. 4(a). With an average of 75%, the spectral extraction efficiency has been achieved for the hexagonal packing type. The following points to be noted. The micropattern introduced onto the glass substrate (they don't induce any alteration either in the architecture of the device or in the functioning) to outcouple

more photons that were trapped mostly in conventional OLED in substate mode due to the combined effect of TIR and waveguiding at boundaries of different refractive index materials. Thus, many rays are emitted from the OLED point in any direction and have further polarization. Fig. 4(b) compares EQE as a function of array height with keeping the aspect ratio constant. The EQE increases monotonically with the microlens array's height and appears to saturate for a higher value of microlens height. It means that a "perfect" microlens array may not be necessary for practical applications. In particular, we are at the following results; firstly, the extraction efficiency depends upon the aspect ratio of an array (aspect ratio defined as the height of the considered array divided by their radius). Secondly, the light extraction efficiency can enhance by outcoupled more photons trapped inside the bottom-emitting OLEDs substrate due to the TIR at the glass/air interface. Tertiary, if all incident rays are perpendicular to the lens's surface, TIR does not occur according to simple ray optics. The light generated inside the device is efficiently coupled to the substrate. Light now traverses through the microlens array without any deflection [26, 27]. The comparison of device performance parameters such as external quantum efficiency of different packing types onto a glass substrate of OLED device as a function of luminance characteristics of three separate arrays on the top of OLED as an external scattering structure is shown in fig—4 (c). Notably, from the figure that the hexagonal array exhibits the highest EQE, 35% (32% Rectangular MLA), then another array (which is higher than 34% EQE reported in the literature [16]). While the roll-off takes place with a minimum reached EQE 30% at the brightness level of 10^5 lm/m^2,

Fig. 5 shows the angular-dependent E.L. spectra of OLED devices attached with different microlens micropattern arrays as a wavelength function. The El spectrum has two peaks because of the singlet and the second due to triplet transition due to the attribution of two primary colors that function as a phosphorescent active layer. The E.L. spectrum shows the two peaks at wavelength 512 nm and 600 nm. The emission curve shows a slight shoulder band around 650 nm as the peak intensity corresponds to exciton dynamics. Hence, the corresponding maximum generation of an exciton exhibits in hexagonal packing type. It has been observed that the intensity of the first peak is greater than the second peak, which means that electrically generated triple excitons can be exchanged via crossing the EML1 and transferring the Dexter energy from the EML2. Firstly, the following points to note: Due to reduced electrons' reduced repulsion, a singlet exciton's energy is more significant than a triplet exciton's energy. Secondly, due to a different pair of spin properties, singlet to triplet transition involves a change in the electronic state. Due to the following reason, the singlet state lifetime is less than that of the triplet state [13, 28]

Fig. 6(a, b) displays the angular dependent CIE coordinates of the OLED device attached with/without a hexagonal or rectangular microlens array. The CIE x index of a device without microlens array decreased first and then increased, see fig. 6(a) while the CIE y index first increased then dropped, see fig. 6(b). In the studied range of viewing angle, the maximal variations of the CIE x and CIE y panel indices were 0.0621 and 0.0768, respectively. However, when the OLED device was attached with a microlens array with packing type hexagonal or rectangular, the CIE x index decreased, and the CIE y index increased initially and then decreased with increasing the viewing angle. Table III illustrates the angular dependent CIE x

and CIE y indices maximum variations (i.e., the difference between maximum and minimum values). More considerable variation in the CIE x and CIE y index values are observed for OLED devices without microlenses array in the calculated range of viewing angle. This suggested that the OLED device connected with either hexagonal or rectangular microlenses is also more sensitive than the OLED device without microlenses to the viewing angle range [20, 21].

Table III. Angular dependent CIE indices maximal variation of the OLED device attached with/without hexagonal or rectangular microlens arrays

Item	Without microlens	Hexagonal microlens arrays	Rectangular microlens arrays
$(CIE\ X)_{max}$ - $(CIE\ X)_{min}$	0.0621	0.0381	0.0331
$(CIE\ y)_{max}$ - $(CIE\ y)_{min}$	0.0768	0.0190	0.0205

The Comparisons of outcoupled efficiency as a function of ETL-TPBi thickness of OLED attached with microlens arrays, in which the orientation of point dipole was set up as isotropic (fig 7(a)), T.M. (fig 7(b)), and T.E. (fig 7(c)) polarization mode concerning the interface. All three-polarization mode shows an oscillation pattern in air medium with radiative quantum efficiency value as 0.6. The governing oscillation pattern in all three-mode due to the multi-beam interference effect, i.e., it is a difference in optical path length and phase shift that occurred throughout the reflection at the metal cathode, the electron transport layer thicknesses. Therefore, the photons generated in the active layer propagate toward the HTL, ITO, glass substrate, and out of the device. Part of them propagate toward the metal cathode and reflect back [31]. Hence, the emissive dipole moment's orientation significantly impacts the outcoupling efficiency as the proportion of light trapped within the OLED in parasitic waveguide mode. As a result, the OCE strength sinusoidally decreased with ETL thickness. The orientation of point dipole was set up as isotropic concerning the interface, see fig. 7(a). The first maxima with the highest OCE observed for the hexagonal array at 70 nm and 220 nm second maxima for air medium. The strength of oscillations decreases as the distance rises due to reduced dipole radiation intensity with increasing distance from the dipole. The intensity of the outcoupling efficiency is thus reduced by increasing the thickness of ETL. However, we found a higher value of OCE (for ETL-50 nm, see fig. 7(b)) than the transverse electric mode, i.e., perpendicular polarization (ETL 180 nm, see fig. 7(c)) in point dipole orientation. Thus, the emitter's dipole orientation is essential if OLEDs' light emission characteristics are determined. The TM mode provides more performance efficiency than the T.E. in the air because OCE has the main concern with the air mode, i.e., how much light has come out of the system and is stuck in a parasite mode [13, 19, 29].

4. Conclusion

In summary, a simulation approach is used to enhance the light extraction efficiency by utilizing hexagonal or rectangular microlenses array onto the glass substrate of OLED devices. The device with hexagonal packing type exhibits the highest EQE up to 35% at 103 lm/m2 brightness level and with minimum roll-off in EQE 30% take place at the brightness level of 105 lm/m2. The variation of luminance with viewing angle decreased as we moved toward the normal direction with a minimum enhancement in luminance 83.4% at 60 degrees for the hexagonal array. A wider FWHM was observed in the E.L. spectrum. Concurrently, we also correlate the change in OCE for different dipole orientations and are seen as more sensitive in horizontal polarization mode. From the CIE x and CIE y index studied, we observed that the OLED device connected with either hexagonal or rectangular microlenses array is more sensitive than the OLED device without microlenses to the viewing angle range. Finally, the simulation outcomes showed that the addition of microlens packing types on the top of the OLED device significantly enhanced light extraction efficiency and provided better results for device fabrication

Declarations

Conflict of Interest

The authors declare that they have no conflict of interest.

Acknowledgment

References

1. K. Leo, Nat. Photonics, **5,** 716(2011).
2. Joan Ràfols-Ribé, Paul-Anton Will, Christian Hänisch, Marta Gonzalez-Silveira, Simone Lenk, Javier Rodríguez-Viejo and Sebastian Reineke, Science Advance, **4**, eaar8332(2018).
3. Rohit Ashok Kumar Yadav, Deepak Kumar Dubey, Sun-Zen Chen, Tzu-Wei Liang & Jwo-Huei Jou, Sci. Rep. **10** (1) (2020) 9915.
4. R. Bathelt, D. Buchhauser, C. Gärditz, R. Paetzold, P. Wellmann, Organ. Electron. **8** 293(2007).
5. Johnson, Aaron and Lee, Shu-Jen and Klein, Julien and Kanicki, Jerzy, J. Rev. Sci. Instrum. **78,** 096101 (2007).
6. Cheol Hwee Park, Jae Geun Kim, Sun-Gyu Jung, Dong Jun Lee, Young Wook Park & Byeong-Kwon Ju, Sci. Rep. **9**, 8690(2019).
7. Hyeck Go, Tae-Wook Koh, Hyunsu Jung, Cheol Young Park, Tae-Won Ha, Eun Mi Kim, Moon Hee Kang, Yong Hyun Kim, Changhun Yun, Org. Electron. **47** 117, (2017).
8. T. W. Koh, J.A. Spechler, K.M. Lee, Craig B. Arnold, and Barry P. Rand, ACS Photonics **2** (9) (2015)1366-1372.

9. Bao Dong To, Hsin Chu Chen, Duc Dung Nguyen, Wen Yung Yeh, Jeng-Rong Ho, Hung-Chih Kan, Chia Chen Hsu, Org. Electron. **59** (2018) 164–170.

10. Hyungchul Bae, Jun Soo Kim, Chinsoo Hong, Optics Communications, **415**, 168(2018).

11. Kejun Zhong, Yanjun Fu, Guangyu Jiang, Optik, **212**, 164604(2020).

12. Junji Kido, Masato Kimura, Katsutoshi Nagai, Science, **267,** 1332 (1995).

13. Arvind Sharma T. D. Das, Optik, **221**, 165350 (2020).

14. Zhongbin Wu, Ning Sun, Liping Zhu, Hengda Sun, Jiaxiu Wang, Dezhi Yang, Xianfeng Qiao, Jiangshan Chen, Saad M. Alshehri, Tansir Ahamad, and Dongge Ma, ACS Appl. Mater. Interfaces, **8,** 3150(2016).

15. Yanping Wang, Wenjie Wang, Zhaoji Huang, Huahang Wang, Junting Zhao, Jinhua Yu and Dongge Ma, J. Mater. Chem. C., **6,** 7042(2018).

16. Francesco Galeotti, Wojciech Mróz, Guido Scavia, Chiara Botta, Organic Electronics 14 (2013) 212–218.

17. M. Mesta, M. Carvelli, R. J. de Vries, H. van Eersel, J. J. vander Holst, M. Schober, M. Furno, B. Lüssem, K. Leo, P. Loebl, R. Coehoorn, and P. A. Bobbert, Nat. Mater.**12**, 652(2013).

18. Cheol Hwee Park, Jae Geun Kim, Sun-Gyu Jung, Dong Jun Lee, Young Wook Park & Byeong-Kwon Ju, Scientific Reports, **9**, 8690(2019).

19. Arvind Sharma, T. D. Das, Optical and Quantum electronics, **53**, 83(2021).

20. Jiun-Haw Lee, Yu-Hsuan Ho, Kuan-Yu Chen, Hoang-Yan Lin, Jheng-Hao Fang, Sheng-Chih Hsu, Jia-Rong Lin, and Mao-Kuo Wei, Optics Express, **16,** 21184(2009).

21. Arvind Sharma, Sagar Bhattarai, T. D. Das, AIP Conference Proceedings **2269**, 030049 (2020).

22. Y. C. Chen, C. T. Pan, C. C. Hsieh, C. Y. Su, H. C. Wu, W. C. Li, Journal of Nanomaterials, vol. 2013, Article ID 797534, 6 pages, 2013.

23. Stéphane Altazin, Lieven Penninck, and Beat Ruhstaller, "Outcoupling technologies: concepts, simulation, and implementation", in Handbook of Organic Light-Emitting Diodes, edited by C. Adachi, R. Hattori, H. Kaji, and T. Tsujimura (Springer Japan, Tokyo, 2019), DOI: https://doi.org/10.1007/978-4-431-55761-6_21-1.

24. S. Möller and S. R. Forrest, Journal of Applied Physics **91**, 3324 (2002).

25. Rahul K. Sharma, Deepak and Monica Katiyar, Organic Electronics, **38,** 121(2016).

26. Wang, Yanping and Wang, Wenjie and Huang, Zhaoji and Wang, Huahang and Zhao, Junting and Yu, Jinhua and Ma, Dongge, J. Mater. Chem. C **6,** 7042(2018).

27. Feng, Jing and Liu, Yue-Feng and Bi, Yan-Gang and Sun, Hong-Bo., Laser & Photonics Reviews, **11**, 1600145(2017).

28. Hajime Nakanotani, Takahiro Higuchi, Taro Furukawa, Kensuke Masui, Kei Morimoto, Masaki Numata, Hiroyuki Tanaka, Yuta Sagara, Takuma Yasuda & Chihaya Adachi, Nature Communications **5**, 4016 (2014).

29. Arvind Sharma, T. D. Das, Material today Proceedings, https://doi.org/10.1016/j.matpr.2020.10.882. (2020).
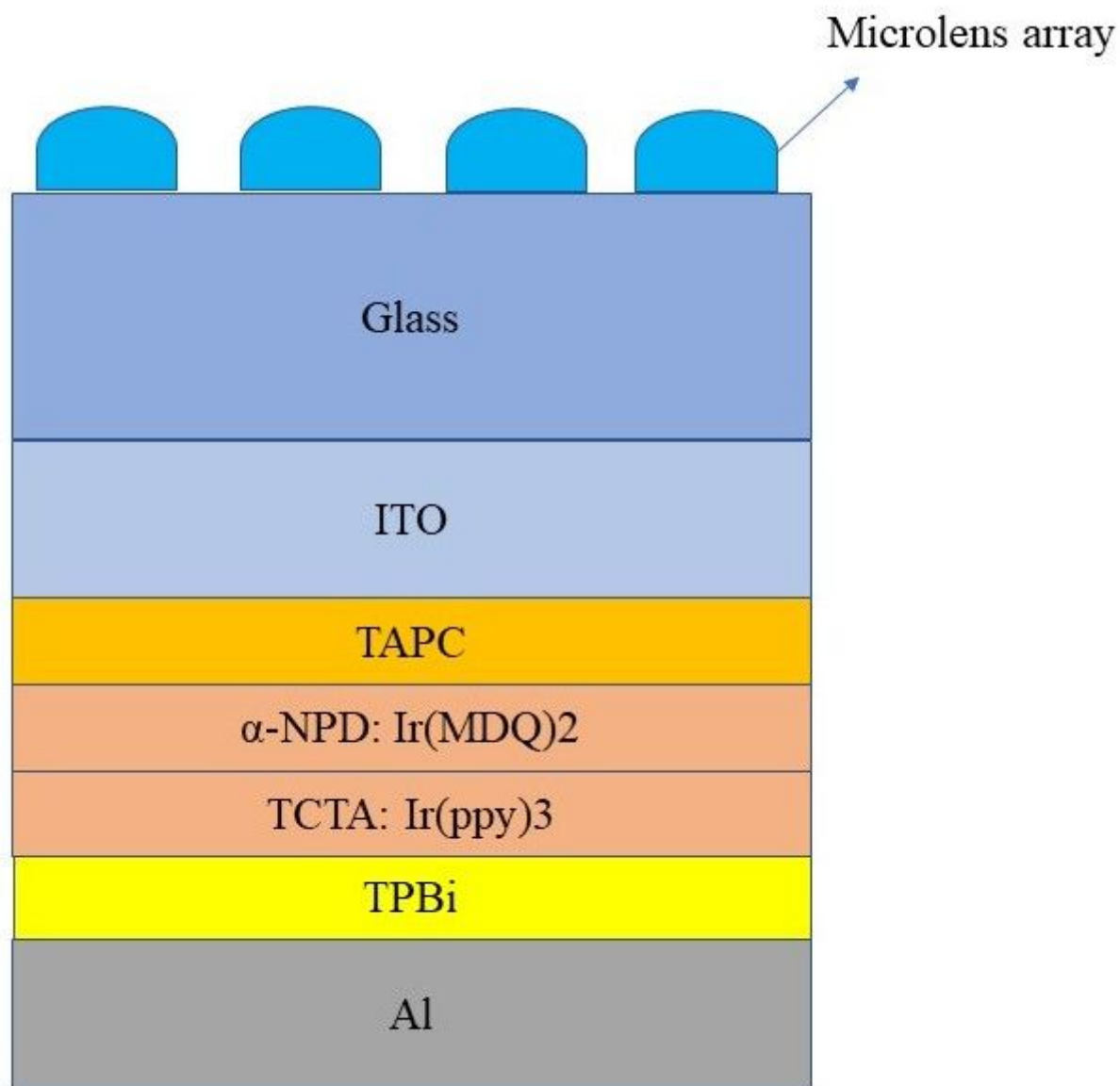
Figures

Figure 1

(a) Pictorial representation of dual scheme OLED device with a microlens array as an external scattering structure (b) microlens array three-dimensional view; the green lines reflect the outgoing rays, and the blue lines reflect the incident rays.
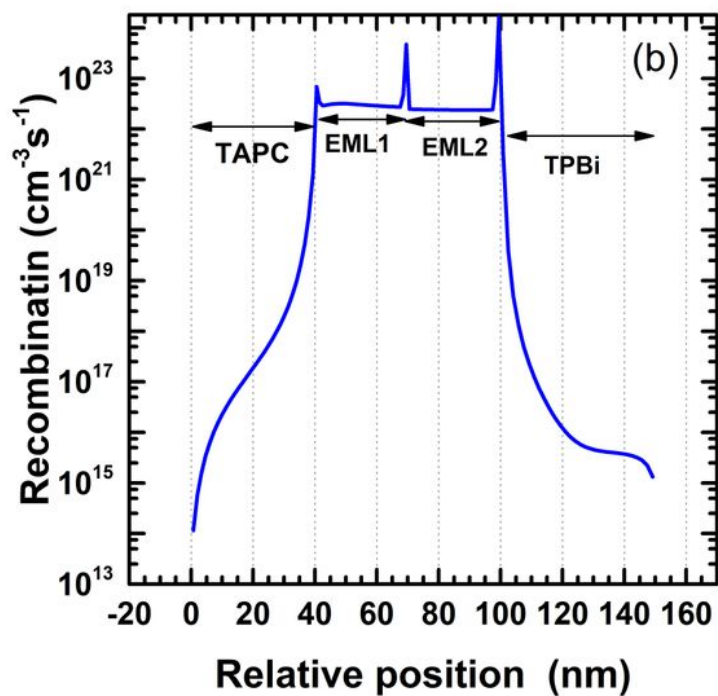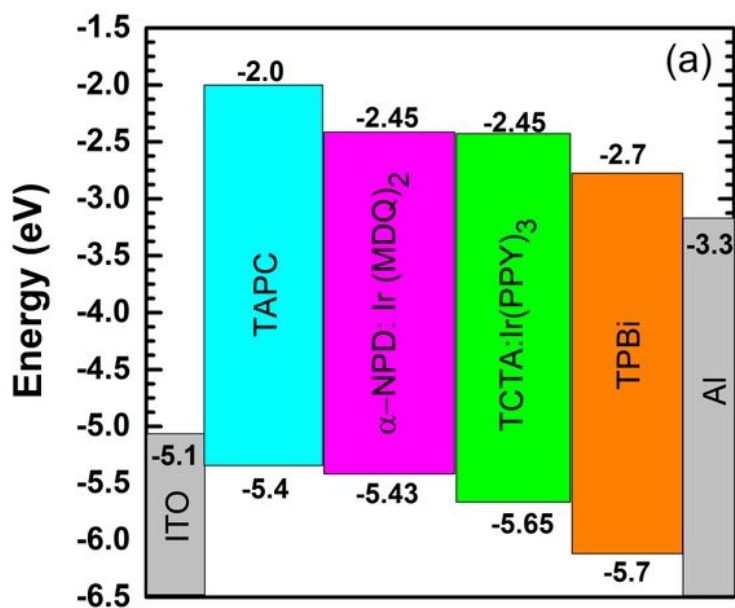
Figure 2

(a) Energy level alignment diagram of dual scheme OLED device (b) represents the recombination zone distribution.
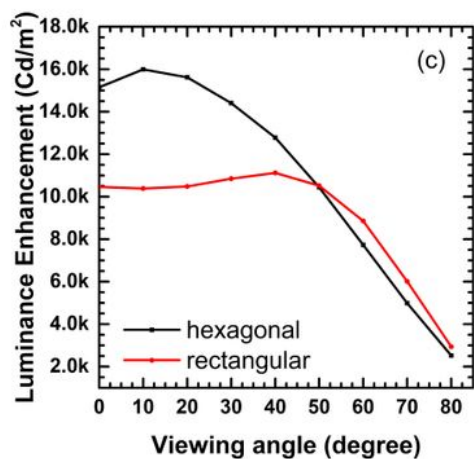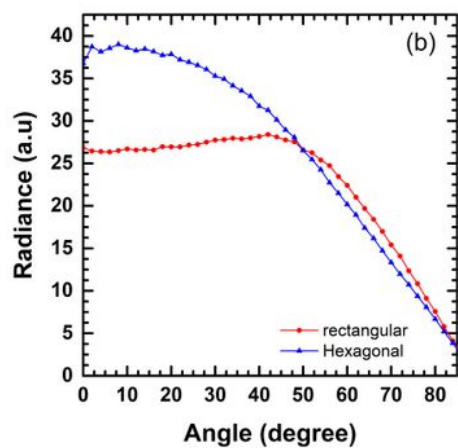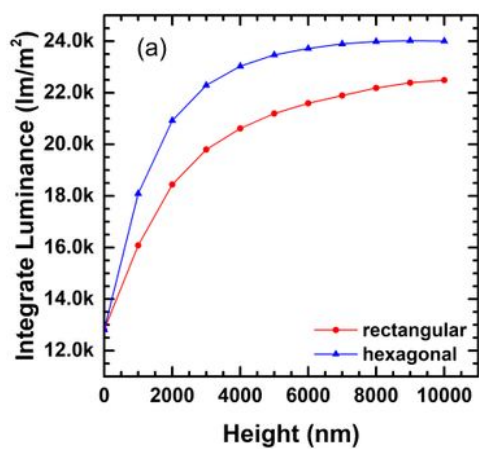
Figure 3

Comparing different microlens micropatterns onto a glass substrate of OLED device (a) integrated luminance- the height of the array (b) luminance-viewing angle relation, keep aspect ratio constant.
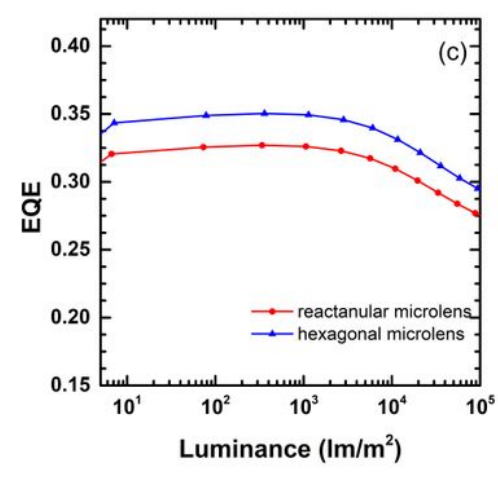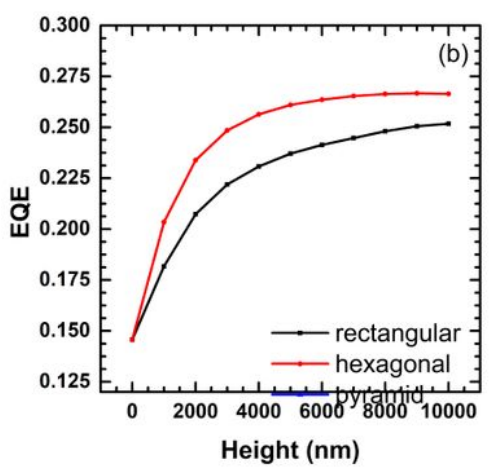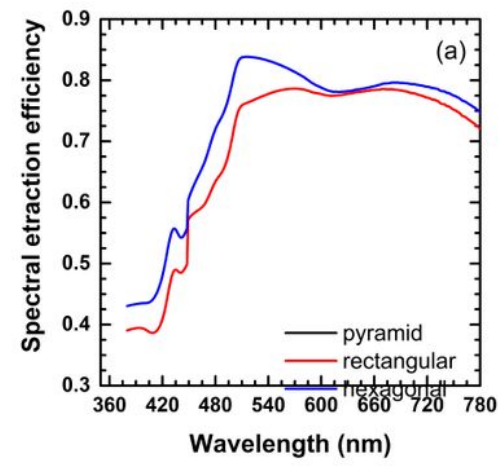
Figure 4

Comparison of device performance parameters such as external quantum efficiency of different microlens micropattern onto a glass substrate of OLED device (a) spectral extraction efficiency-wavelength (b)EQE-height of an array (c) EQE-luminance characteristics.
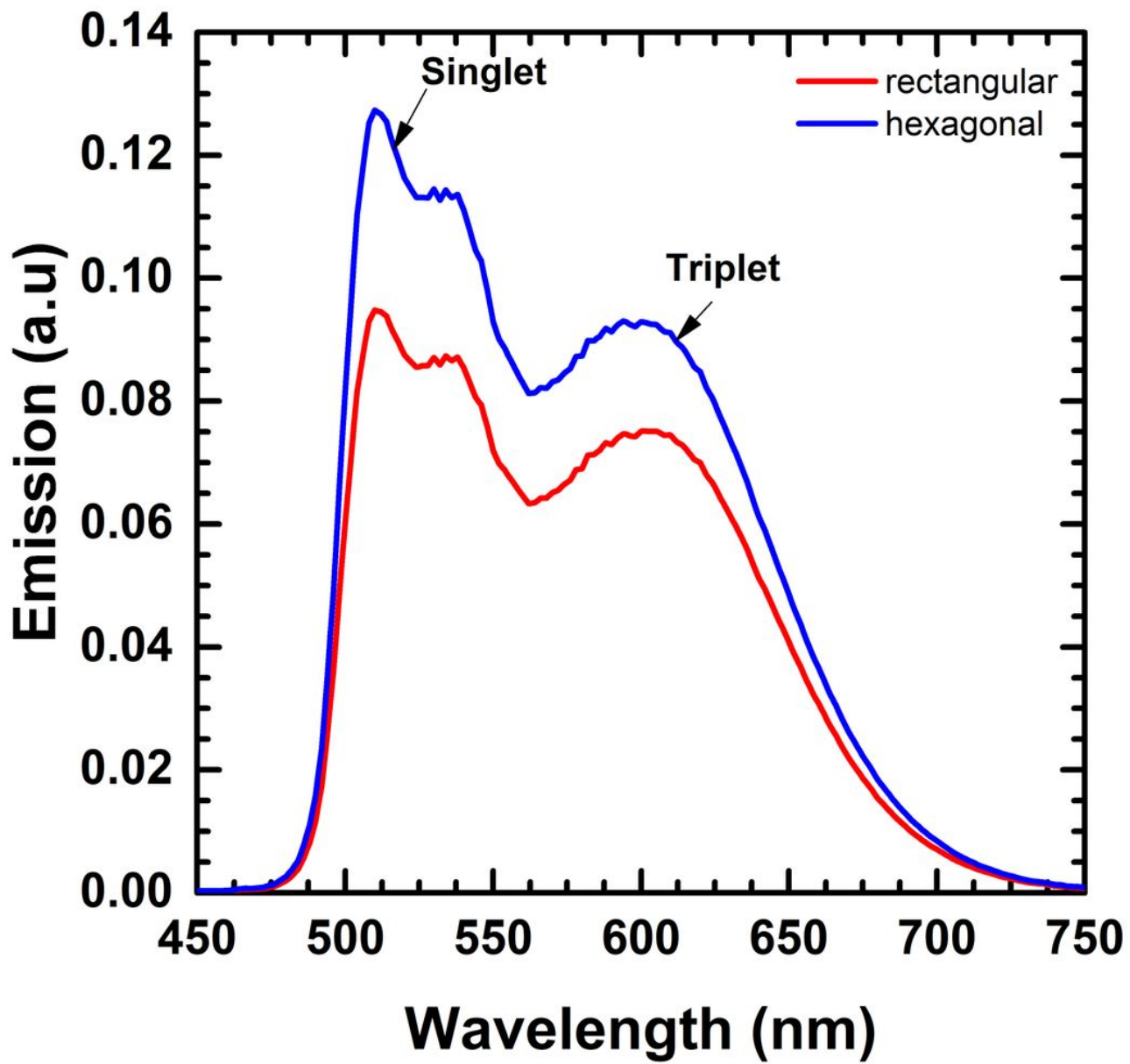
Figure 5

The Electroluminance spectrum is dependent on the viewing angle of different microlens micropattern arrays at a default angle of 30 degrees.
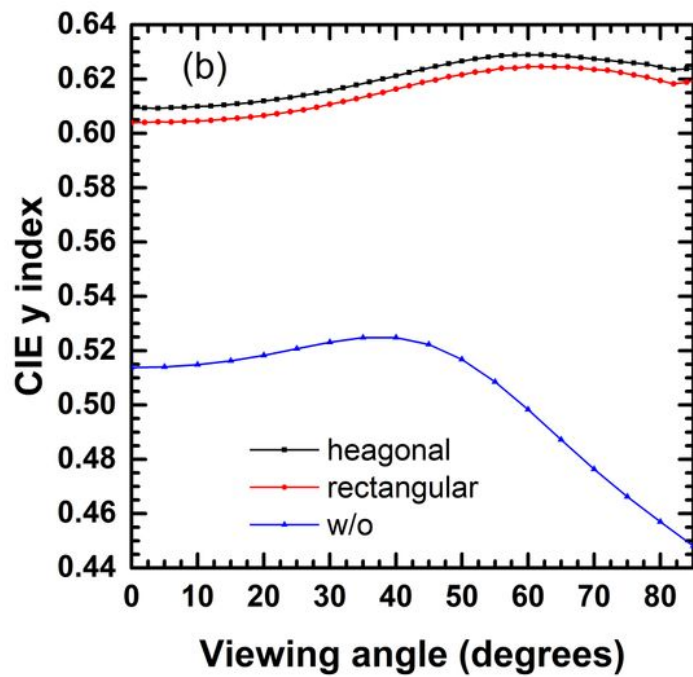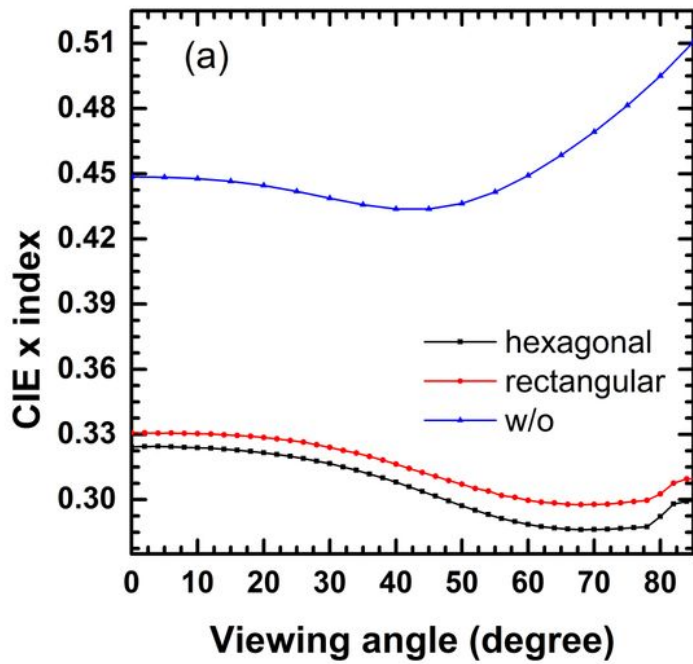
Figure 6

The OLED device's CIE coordinates are attached with/without a hexagonal or rectangular microlens array at different viewing angles.
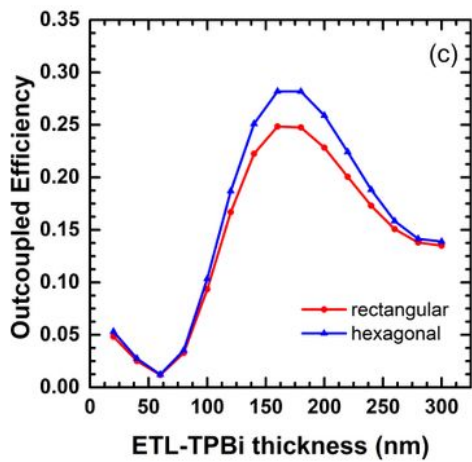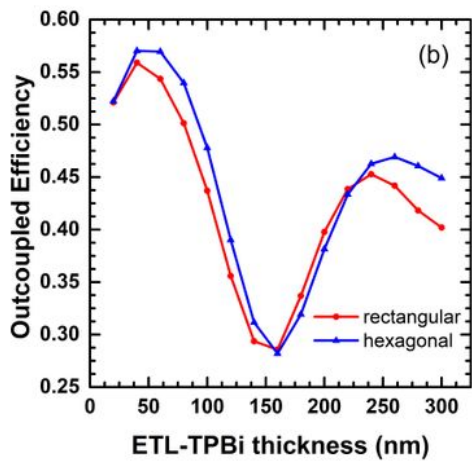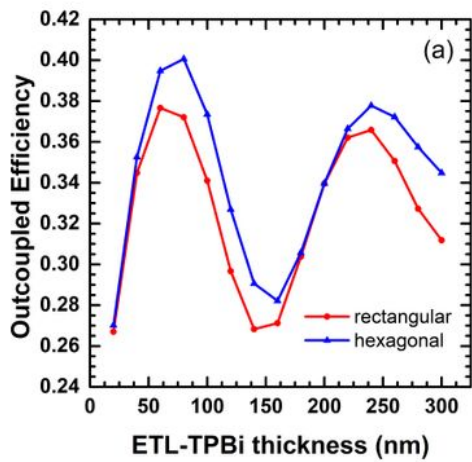
Figure 7

Comparisons of integral emission into the air as a function of electron transport layer thickness of three different micropattern array with radiative quantum efficiency as 0.6 (a) isotropic (b) horizontal (c) vertical polarization.